Journal of Applied Mechanics and Technical Physics, Vol. 42, No. 5, pp. 851–856, 2001

CONJUGATE HEAT EXCHANGE AND HYDRODYNAMICS FOR A VISCOUS INCOMPRESSIBLE FLUID MOVING IN A RECTANGULAR CAVITY

G. V. Kuznetsov and A. V. Krainov

UDC 536.2:532/533; 532.516

Numerical simulation was performed of the motion of a viscous incompressible nonisothermal fluid in an open rectangular cavity under conditions of forced convection and conjugate heat exchange. The effect of the jet dynamic parameter (Reynolds number) and fluid flow conditions on the character of motion and heat exchange of viscous incompressible nonisothermal fluids in rectangular cavities is studied. A hydrodynamic pattern of viscous flow in an open cavity under forced convection conditions (in the conjugate and nonconjugate formulations of the problem) is obtained. The effect of parameters of the model on the character of motion is studied. Temperature profiles for the solid and fluid phases are obtained. The effect of parameters of the model on the character of temperature distribution in both phases is studied.

Introduction. Over the past forty years there has been steady interest in convective flows in cavities of various types, which is explained by the practical importance of the problem: cavities are used as heat-transferring, heat-insulating, and structural elements in power and process installations of various purposes, electronics, and heat exchangers [1, 2].

Studies of the frontal interaction of a viscous incompressible nonisothermal jet with a variously shaped bounded volume is of great scientific and practical significance because such flows are widely used in engineering processes of various complexity levels in metallurgical, power, etc., industries [2–5].

Simulation of heat exchange for a viscous flow in a rectangular cavity involves solution of complex problems of forced convection of an incompressible fluid. Since the complexity of viscous incompressible nonisothermal flows in bounded volumes makes it impossible to develop reliable analytical methods to calculate such flows, numerical simulation is required.

Formulation of the Problem. We consider the unsteady interaction of a subsonic laminar viscous jet of an incompressible nonisothermal fluid with an open rectangular cavity (Fig. 1). Numerical solution of the hydrodynamic problem was implemented in region 2, bounded by the inflow region 1, the line of symmetry 3, the side wall 6, the bottom of the cavity 4, and the region of exit 7 from the rectangular cavity.

We use a mathematical model based on the Navier–Stokes equations in the variables "vortex–stream function" at moderate Reynolds numbers ($100 \leqslant \mathrm{Re} \leqslant 800$), the energy equation, and the heat-conduction equation for the material of the rectangular cavity with corresponding initial and boundary conditions:

$$\frac{\partial\omega}{\partial\tau} + u\frac{\partial\omega}{\partial x} + v\frac{\partial\omega}{\partial y} = \frac{1}{\mathrm{Re}}\Big(\frac{\partial^2\omega}{\partial x^2} + \frac{\partial^2\omega}{\partial y^2}\Big), \qquad \frac{\partial^2\psi}{\partial x^2} + \frac{\partial^2\psi}{\partial y^2} = \omega,$$
$$\frac{\partial\theta}{\partial\tau} + u\frac{\partial\theta}{\partial x} + v\frac{\partial\theta}{\partial y} = \frac{1}{\mathrm{RePr}}\Big(\frac{\partial^2\theta}{\partial x^2} + \frac{\partial^2\theta}{\partial y^2}\Big), \qquad \frac{\partial^2\theta_1}{\partial x^2} + \frac{\partial^2\theta_1}{\partial y^2} = \frac{\partial\theta_1}{\partial \mathrm{Fo}}. \tag{1}$$

Here Pr and Fo are the Prandtl and Fourier numbers, respectively.

At the bottom of the cavity ($y = S$ and $D < x < L$), we specify nonpenetration and attachment conditions and the boundary condition of the fourth kind for the energy equation:

Institute of Applied Mathematics and Mechanics, Tomsk State University, Tomsk 634050. Translated from Prikladnaya Mekhanika i Tekhnicheskaya Fizika, Vol. 42, No. 5, pp. 136–143, September–October, 2001. Original article submitted December 18, 2000; revision submitted March 20, 2001.

0021-8944/01/4205-0851 $25.00

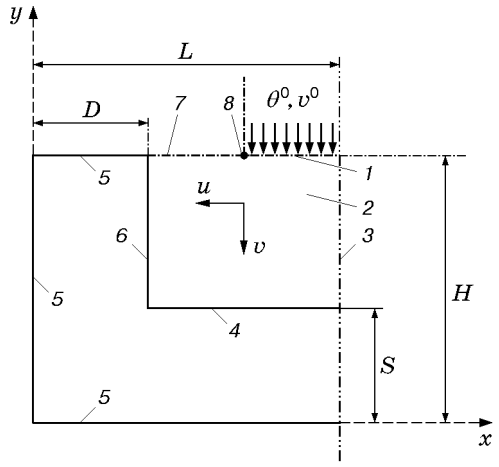

Fig. 1. Diagram of the flow in a rectangular cavity and geometry of the computation domain: 1) entrance to the cavity; 2) hydrodynamic region; 3) symmetry axis; 4) bottom of the cavity; 5) outer walls of the cavity; 6) side wall of the cavity; 7) region of exit from the cavity; 8) boundary between the exit and entrance regions.

$$\psi = 0, \quad \omega = 2\,\frac{\psi(x, y+\Delta y)}{(\Delta y)^2}, \quad \theta_1 = \theta, \quad \lambda_1\,\frac{\partial\theta_1}{\partial y} = \lambda\,\frac{\partial\theta}{\partial y}. \tag{2}$$

On the side wall of the cavity ($x = D$ and $S < y < H$) the same conditions are imposed:

$$\psi = 0, \quad \omega = 2\,\frac{\psi(x+\Delta x, y)}{(\Delta x)^2}, \quad \theta_1 = \theta, \quad \lambda_1\,\frac{\partial\theta_1}{\partial x} = \lambda\,\frac{\partial\theta}{\partial x}. \tag{3}$$

On the symmetry axis of the jet ($x = L$ and $S < y < H$), we specify the conditions of heat-flux continuity and nonpenetration

$$\frac{\partial\psi}{\partial x} = 0, \quad \omega = 0, \quad \lambda\,\frac{\partial\theta}{\partial x} = 0. \tag{4}$$

At the exit from the rectangular cavity, we use the "drift" conditions $\partial u/\partial y = 0$ and $\partial v/\partial x = 0$ for the velocity components and a "soft" boundary condition for the temperature (zero second derivative of temperature with respect to y) [6, 7]. On the outer boundaries of the cavity, heat insulation conditions are specified:

$$\begin{aligned}
&y = H, \quad 0 < x < D: && \lambda_1\,\frac{\partial\theta_1}{\partial y} = 0,\\
&y = 0, \quad 0 < x < L: && \lambda_1\,\frac{\partial\theta_1}{\partial y} = 0,\\
&x = 0, \quad 0 < y < H: && \lambda_1\,\frac{\partial\theta_1}{\partial x} = 0,\\
&x = L, \quad 0 < y < S: && \lambda_1\,\frac{\partial\theta_1}{\partial x} = 0.
\end{aligned} \tag{5}$$

In the fluid flow in the cavity, two regions are distinguished: the entrance to the cavity 1 and the exit from the cavity 7 (Fig. 1). The position of the point of separation of the entrance and exit regions is found from the following integral relation, which defines the flow rate as the main integral characteristic of the flow:

$$\int_{x_2}^{x_0} v_+(x, y)\,dx = \int_{x_0}^{x_1} v_-(x, y)\,dx.$$

Here x_1 is the fixed extreme point of the entrance region that lies on the symmetry axis, x_0 is the coordinate of the point of separation of the regions with different fluid flow directions in the cavity ($x_2 < x_0 < x_1$), x_2 is the coordinate of the fixed extreme point of the exit region that lies on the side wall of the cavity, $v_-(x, y)$ is the transverse component of the fluid velocity in the direction from the entrance to the bottom of the cavity, $v_+(x, y)$ is the transverse velocity component of the fluid flow in the direction from the bottom of the cavity to the exit region.

TABLE 1

Grid	[7, 8]			Present work		
	x	y	ψ_*	x	y	ψ_*
Re = 300						
20×17	0.342	0.375	0.043	0.352	0.386	0.044
39×33	0.316	0.359	0.051	0.325	0.369	0.052
Re = 500						
20×17	0.342	0.375	0.036	0.352	0.386	0.037
39×33	0.302	0.328	0.050	0.311	0.337	0.051

The initial conditions are written as

$$\psi(x, y, 0) = \psi^0(x, y), \qquad \theta(x, y, 0) = \theta^0(x, y). \tag{6}$$

The Navier–Stokes equations in the variables "stream function–vortex," the energy equation, and the heat-conduction equation [Eqs. (1)–(6)] are solved by the finite-difference method. The difference analogs of the Navier–Stokes equations are solved by the explicit iterative method of [8]. The difference analogs of the energy equations and thermal-conduction equations are solved by the sweep method [7–9]. A difference scheme of second-order accuracy was used. The calculations were performed on a uniform difference grid.

In the formulation of the problem for the Navier–Stokes equations in the variables "vortex–stream function," the boundary conditions for the solid fixed surface have the form [7, 8]

$$\psi = 0, \qquad \frac{\partial \psi}{\partial \boldsymbol{n}} = 0, \tag{7}$$

where $\boldsymbol{n}$ is the normal line to the solid surface.

In the numerical solution of the difference equation for vortex, boundary conditions for it need to be determined because boundary conditions (7) relating to the Navier–Stokes equations are specified only for the stream function and not for the vortex.

In the present study, we used a method in which the stream function near the boundary is written as a Taylor series. This gives the expression for the vortex on the boundary [6].

Test Problems. To test the approximation and convergence of the numerical solution, we used the problem of a two-dimensional flow in a rectangular cavity with the upper wall moving in its plane with constant velocity [6–9].

Profiles of the longitudinal $[u(y)]$ and transverse $[v(y)]$ velocity components are determined. Stream functions are calculated for various values of the Reynolds number $300 \leqslant \mathrm{Re} \leqslant 1000$ and various numbers of nodes of the difference grid $20 \leqslant m_1 \leqslant 60$ and $17 \leqslant m_2 \leqslant 60$ (m_1 and m_2 are the numbers of grid nodes along the x and y coordinates, respectively). The results obtained differ from the results of [6–8] by not more than 7%. Table 1 gives maximum values of the stream function ψ_* and the x and y coordinates of the points at which these values are reached for Re = 300 and 500 on grids 20×17 and 39×33.

As a second test problem, we solved the problem of shear circulation flow at small Reynolds numbers $10 \leqslant \mathrm{Re} \leqslant 50$, which reduces to solving a biharmonic equation for the stream function [10–12]. The stream function profiles obtained differ from the results of [10] by not more than 5%.

Results and Discussion. Flows of various fluids, in particular, water, molten lead, and fluid steel were studied over a wide range of Reynolds numbers and other parameters of the model. Figures 2–4 show numerical results for fluid steel at a temperature of 1500°C.

As follows from analysis of the steady-state flow field for various values of the geometrical characteristics of the cavity (in particular, $L/H = 1/2$, $2/3$, and 1) over a rather wide range $100 \leqslant \mathrm{Re} \leqslant 500$, the fluid reaches the bottom of the cavity, rotates, and flows out through the entire region 7 (see Fig. 1). Thus, in the viscous incompressible nonisothermal flow in the cavity, we can distinguish two stages.

The first stage includes the passage of the fluid from the entrance region to the bottom of the cavity and interaction with the bottom. The interaction of the jet with the bottom of the cavity is accompanied by deceleration of the flow and occurrence of a region of elevated pressure, which leads to spread of the fluid along the bottom of the cavity.

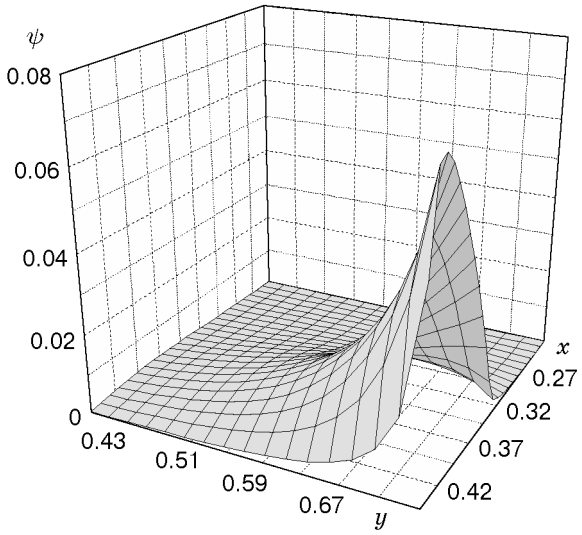

Fig. 2. Distribution of the stream function for steady flow (Re = 200 and $L/H = 2/3$).

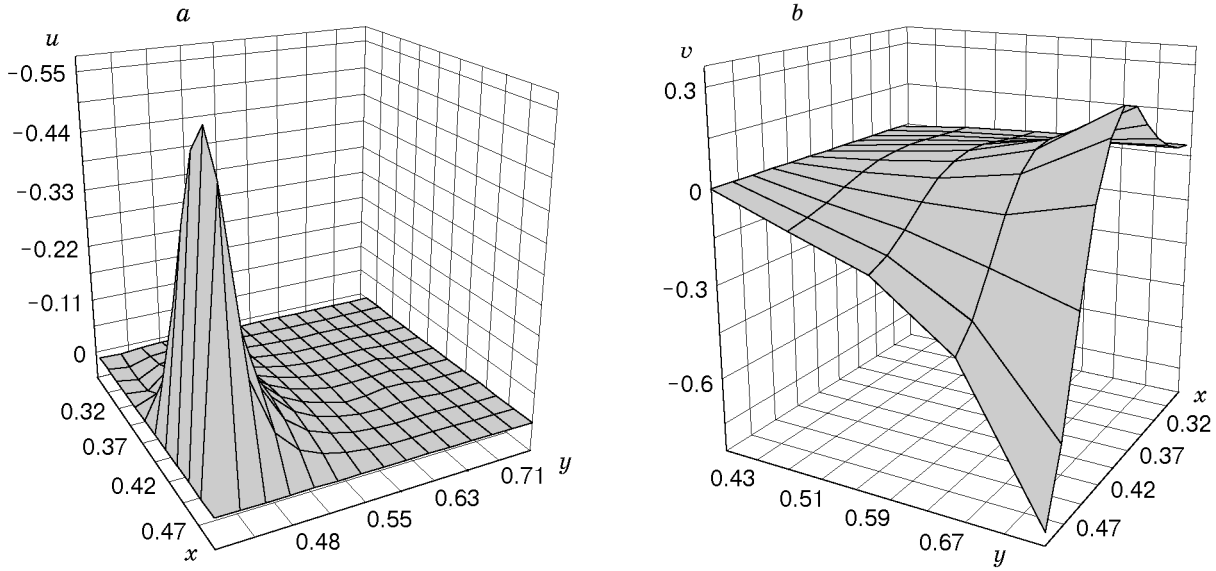

Fig. 3. Distribution of the longitudinal (a) and transverse (b) velocity components for steady flow (Re = 200).

At the second stage, the fluid moves from the bottom of the cavity to the exit with formation of a region of reverse flow. At this stage, deceleration of the fluid continues, which also leads to which a region of elevated pressure arises.

The direct and reverse regions flow corresponding to the above stages of fluid flow in the cavity are evident in Fig. 3b.

Figure 2 shows the distribution of the stream function $\psi(x, y)$ for the time t^* corresponding to the steady-state flow field for Re = 200 and a geometrical ratio of the sides of the cavity $L/H = 2/3$. The maximum value of the stream function is in the region of $0.35 < x < 0.39$, $0.67 < y < 0.75$, in which the most intense formation of vortex structures is observed. We note that the analysis performed revealed the rather strong effect of the geometrical characteristics on the formation of the stream-function field.

Figure 3a gives the distribution of the longitudinal velocity component $u(x, y)$ at the time t^* for Re = 200. The maximum velocity is in the region of $0.40 < x < 0.44$ near the bottom of the cavity. With increase in Reynolds number, the behavior of the longitudinal velocity component remains unchanged.

Figure 3b shows the distribution of the transverse velocity component $v(x, y)$ at time t^* for Re = 200. We note that with increase in Reynolds number, the profile of $v(x, y)$ at the initial sections of the cavity becomes close to a constant value, while at Re = 100 and 200, the profiles of the transverse velocity component are almost parabolic

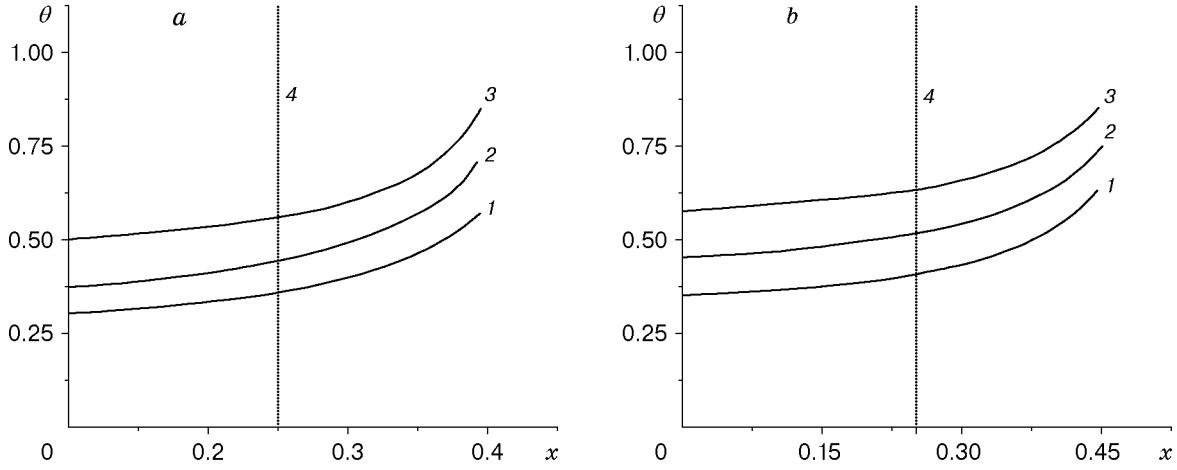

Fig. 4. Solid- and liquid-phase temperature distributions along the x coordinate for steady flow: (a) Re = 300, Pr = 0.979, $a = 0.3a_*$, $L/H = 1/2$, and $y = 0.40$ (1), 0.52 (2), and 0.68 (3); (b) Re = 500, Pr = 0.979, $a = 0.32a_*$, $L/H = 1/2$, and $y = 0.40$ (1), 0.56 (2), and 0.64; curves 4 are interfaces between the liquid and solid phases.

at the same sections. An analysis of the distribution of the transverse velocity component shows that in the flow field, two maxima are formed, which correspond to the direct and reverse flows.

From Fig. 3, it is evident that at the first stage, as the incompressible fluid jet moves to the bottom of the cavity, the transverse velocity component decreases with increase in the longitudinal component, which is clearly seen in the region of $0.41 < y < 0.55$. At the second stage, as the jet moves to the exit section, the longitudinal velocity component decreases, which is clearly seen in the region of $0.32 < x < 0.41$, $0.41 < y < 0.55$. At the same time, the transverse velocity component begins to increase, and its most intense increase is observed in the region of $0.59 < y < 0.75$, $0.30 < x < 0.40$. According to Fig. 3b, the maximum value of the outflow velocity is $v_{\max} = 0.24$.

The motion of the viscous incompressible fluid in the rectangular cavity was studied under conditions of conjugate heat exchange. The temperature dependences in the solid and liquid phases were obtained for various dynamic parameters and variation of the parameter a (a is the length of the entrance region).

Figure 4a shows solid- and liquid-phase temperature profiles at various sections of y at the time t^* for Re = 300, Pr = 0.979, $a = 0.3a_*$ (a_* is the length of the penetrable region of the cavity $y = H$, $D < x < L$), and $L/H = 1/2$. It should be noted that with increase in a and decrease in geometrical parameters, the behavior of temperature fields along the height of the cavity changes insignificantly.

Figure 4b shows solid- and liquid-phase temperature distributions at various sections of y at the time t^* for Re = 500, Pr = 0.979, $a = 0.32a_*$, and $L/H = 1/2$. As can be seen from Fig. 4b, the temperature profile decreases rather rapidly up to the interface $x = 0.25$, whereas the solid-phase temperature varies much more slowly.

From the results obtained it follows that the behavior of the temperature profiles at various sections of the cavity remains unchanged with variation of the parameter Re.

In the present work, we also solved the nonconjugate problem. On the walls of the cavity, we imposed heat insulation conditions (no heat transfer to the cavity walls).

The difference in the temperatures obtained in the conjugate and nonconjugate formulations of the problem is ±23%, which confirms that solving the problem in the conjugate formulation is reasonable.

Conclusions. The results of numerical analysis given here suggest that the range of application of the mathematical apparatus of [7, 8] can be further extended to solve problems of convective flows in open cavities under conditions of jet inflow and conjugate heat exchange. The present work is a continuation of the studies of [8, 9], in which it was first shown that the mathematical tool of [7] can be used to solve problems in the conjugate formulation for regions having more complex geometry than a channel or a streamlined body [13]. Optimization of grid parameters gives stable solutions of problems in regions of more complex geometry than those considered in [7–9].

The present study showed that stable solutions of the problem considered can be obtained over a rather wide range of Reynolds numbers ($100 \leqslant \mathrm{Re} \leqslant 1000$).

REFERENCES

1. G. V. Makhnova, V. V. Ris, and E. M. Smirnov, "Two-dimensional laminar free convection in a cavity having the shape of a square with rounded angles," in: *Free Convection. Heat and Mass Exchange in Chemical Transformations*, Proc. of the IInd National Conf. on Heat Exchange (Moscow, October 26–30, 1998), Vol. 3, Moscow Energ. Inst. (1998), pp. 100–103.
2. M. Flemings, *Solidification Processing*, McGraw-Hill, New York (1974).
3. N. N. Rykalin. A. A. Uglov, and L. M. Anishchenko, *High-Temperature Technological Processes. Thermal Foundations* [in Russian], Nauka, Moscow (1985).
4. G. F. Balandin, *Theory of Molding* [in Russian], Mashinostroenie, Moscow (1979).
5. V. N. Karnozhitskii, *Contact Heat Exchange during Casting* [in Russian], Naukova Dumka, Kiev (1978).
6. L. G. Loitsyanskii, *Mechanics of Liquids and Gases*, Pergamon Press, Oxford–New York (1966).
7. V. M. Paskonov, V. I. Polezhaev, and L. A. Chudov, *Numerical Simulation of Heat- and Mass-Transfer Processes* [in Russian], Nauka, Moscow (1984).
8. V. I. Polezhaev, A. V. Buné, K. G. Dubovik, et al., *Mathematical Simulation of Convective Heat and Mass Exchange Using the Navier–Stokes Equations* [in Russian], Nauka, Moscow (1987).
9. E. L. Tarunin, *Computational Experiment in Problems of Free Convection* [in Russian], Izd. Irkuts. Univ., Irkutsk (1990).
10. T. Shih, *Numerical Heat Transfer*, Hemisphere, Washington (1984).
11. P. J. Roache, *Computational Fluid Mechanics*, Hermosa, Albuquerque (1976).
12. C. A. J. Fletcher, *Computational Techniques for Fluid Dynamics*, Vol. 2, Springer-Verlag, Heidelberg (1991).
13. A. M. Grishin and V. I. Zinchenko, "Conjugate heat and mass exchange between a reactive body and a gas in the presence of nonequilibrium chemical reactions," *Izv. Akad. Nauk SSSR, Mekh. Zhidk. Gaza*, No. 2, 121–128 (1974).